JOURNAL OF APPLIED ELECTROCHEMISTRY 16 (1986) 28–40

Performance of zirconia membrane oxygen sensors at low temperatures with nonstoichiometric oxide electrodes

S. P. S. BADWAL, F. T. CIACCHI

CSIRO, Division of Materials Science, Advanced Materials Laboratory, PO Box 4331, Melbourne, Victoria 3001, Australia

Received 24 December 1984

Sensor tests on zirconia membrane probes incorporating nonstoichiometric oxides of the general formula (U, M)$O_{2\pm x}$ and having the fluorite structure have been described over the temperature range of 300 to 600° C and oxygen concentrations between 100 and 0.1%. The results have been compared with those for porous platinum electrodes. The sensors with (U, M)$O_{2\pm x}$ electrodes performed well, down to 350° C, whereas those with porous platinum electrodes showed large deviations from Nernstian behaviour even at 450° C. The variables studied included the effect of dopant concentration and type, surface area of the electrode and heat treatment. The electrolyte used in the sensor tests had at least an order of magnitude lower conductivity compared with the traditionally used electrolytes such as Y_2O_3–ZrO_2 or Sc_2O_3–ZrO_2. Despite this, the better performance of sensors provided with (U, M)$O_{2\pm x}$ electrodes suggests that the electrode/electrolyte interface plays a much more dominant role than the electrolyte.

1. Introduction

Several Nernst sensors based on oxygen ion conducting solid electrolytes have been developed in the past for increased fuel efficiency and better control of industrial processes [1–3]. Commercially available oxygen sensors with porous platinum electrodes cannot be used below about 500 to 600° C. When used in automotive applications (350 to 900° C), these sensors can only monitor air/fuel ratio close to stoichiometric and they do not operate accurately on the lean side where maximum fuel economy is envisaged. Other applications such as monitoring of oxygen in the combustion products of domestic/industrial boilers and kilns also require oxygen sensors which are capable of low temperature (400° C or below) operation. Many approaches to lower the operating temperature of the Nernst sensor have failed mainly because of (i) the poor understanding of the nature of charge transport processes within the solid electrolyte cell and (ii) too much emphasis had been put on means of improving the electrolyte conductivity (or conductance-use of thin films etc.)

A close scrutiny of the literature, and examination of charge transport processes in solid electrolyte cells in our laboratory, clearly reveals that:

(a) in a typical Pt/stabilized zirconia/Pt cell it is the electrode resistance which dominates at low temperatures as illustrated in Fig. 1 for one such cell over the temperature range 500 to 750° C;
(b) the time constants associated with the electrode reactions are normally several orders of magnitude higher than that for oxygen ion migration within the defect lattice of an electrolyte [4, 5] indicating that the equilibrium at the electrode/electrolyte interface is more difficult to achieve;
(c) the use of better oxygen ion conductors such as doped ceria and bismuth oxide has not led to noticeable improvements in the

0021–891X/86 $03.00 + .12

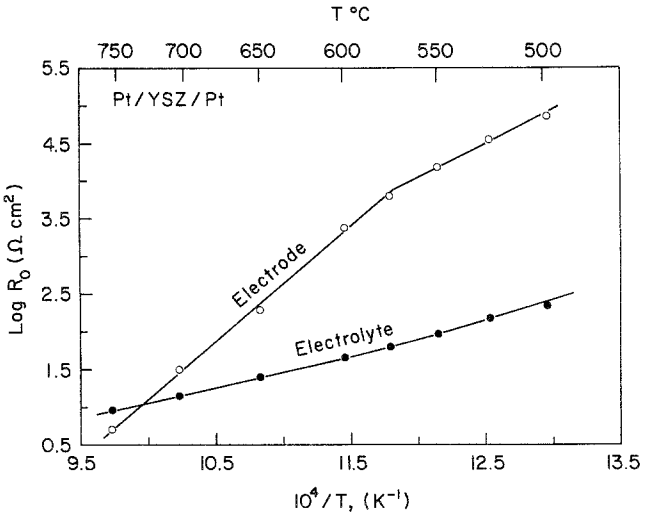

Fig. 1. Arrhenius plots for the electrode, and electrolyte resistance of a typical Pt/Y_2O_3–ZrO_2/Pt cell in 100% oxygen (electrolyte thickness ~ 1.5 mm).

sensor performance at lower temperatures [6, 7];

(d) with noble metal electrodes, especially platinum, the charge transfer reaction is limited to the three phase contact boundary between the electrode, electrolyte and the gas phase. In order to maximize the extent of the three phase boundary and hence charge transfer rates, the platinum should be in finely divided form. This indeed is the case for freshly deposited electrodes (pastes or sputtered). However, it is difficult to retain this finely porous microstructure. Platinum particles tend to coarsen and crystallize on exposure to moderate (~ 600° C) to high temperatures (> 800° C). This results in a decrease of the three phase contact boundary and an increase in the electrode resistance and relaxation time [8, 9]. Other noble metals undergo similar changes on exposure to higher temperatures [10]. The resulting change in the microstructure with consequent loss of electrode activity has a significantly detrimental influence on the minimum operating temperature of oxygen sensors.

Moreover, it is well known that the equilibration of the constituents of incomplete combustion products and development of mixed potentials are characteristic properties of the electrode [1, 11–13] and not those of the electrolyte.

The above observations should not be taken to suggest that the electrolyte conductivity has no effect on the sensor performance. In fact, the e.m.f. drifts and offsets observed at low temperatures have been attributed to grain boundary blocking of oxygen vacancies [14]. These e.m.f. offsets are much lower than those observed at the electrode/electrolyte interface, consistent with the fact that the relaxation times associated with the space charge phenomena at grain boundaries are lower compared with electrode reactions.

The bulk of the evidence suggests that the electrode/electrolyte interface plays an important role in determining the low temperature performance of oxygen sensors. Recent kinetic and microstructural studies on several noble metals and fluorite solid solutions of the general formula (U, M)$O_{2\pm x}$ (M = Sc, Y, Dy, Pr) suggest that the U–M–O solid solutions form an ideal class of electrode materials to be incorporated into low temperature sensors [10, 15–17]. Both the electrode resistance and time constant for the fluorite solid solution electrodes are much lower than those for platinum, especially when the electrodes are heat treated at high temperatures (T > 700° C). The oxygen exchange reaction is most likely occurring over a much larger electrode/electrolyte contact area. The electrodes resist microstructural changes on exposure to higher temperatures and they retain their porous morphology to a larger extent. The

grain size has less influence on the electrode resistance in comparison with noble metals.

This paper describes laboratory tests on sensors incorporating the fluorite solid solution electrodes, in the temperature range 300 to 600° C. The results have been compared with those for porous platinum electrodes. Particular attention was paid to investigating the effects, on the low temperature performance of sensors, of various variables such as:

(a) dopant type and concentration in the (U, M)$O_{2\pm x}$ fluorite solid solution range;
(b) surface area/grain size of the electrode;
(c) heat treatment of electrodes, and
(d) adding increasing amounts of finely divided platinum to the (U,M)$O_{2\pm x}$ solid solution electrodes.

2. Experimental procedures

2.1. *Preparation of sensor bodies*

The sensor bodies were prepared by high temperature (> 1800° C) eutectic welding [18, 19] of solid electrolyte discs of 50 wt % (4.7 mol % Sc_2O_3 + 95.3 mol % ZrO_2) + 50 wt % Al_2O_3 (4.7 ScZAl) composition on to alumina tubes (i.d. = ~5 mm and o.d. = ~8 mm for alumina tubes). The electrolyte discs were 1.5 to 2.0 mm thick and had a diameter of 6 to 7 mm. The sensor bodies produced by this technique are rugged in construction and can withstand high thermal and mechanical shocks in comparison with zirconia tubes. The preparation of the electrolyte, its phase assemblage, microstructure and conductivity have been described in other publications [20, 21]. After welding, the sensor bodies were tested for leaks (at room temperature) at an air pressure of 30 psi (215 kPa). Those with no observable leaks were selected for application of electrodes. The details of leak rate tests, acoustic emission tests to observe cracking patterns of alumina tube, electrolyte and weld junction during thermal cycling of sensor bodies, and thermal expansion behaviour of the electrolyte composition have been described elsewhere [22].

In addition to the sensor bodies described above, two tubes of 7 mol % Y_2O_3 + 93 mol % ZrO_2 composition (i.d. = 7.5 mm, o.d. = 9.5 mm, length = 450 mm) were purchased from Viking Chemicals Ltd (Denmark) and used in two sensor tests.

2.2. *Electrode preparation*

The (U, M)$O_{2\pm x}$ solid solutions were prepared by coprecipitation of the hydroxides with ammonia from a solution containing the required proportions of uranyl and metal salts (M = Sc, Y, Dy, Pr). The coprecipitated powders were dried and calcined in air at higher temperatures. In order to produce small grain size (large surface area) electrodes, the calcination temperatures were generally kept to a minimum consistent with the formation of a single fluorite phase. The completeness of the reaction was detected by taking X-ray diffractograms of the calcined powders. In each case they showed the presence of a single fluorite phase.

In order to study the effect of electrode surface area on the sensor performance, the coprecipitated powder to give $(U_{0.4}Pr_{0.6})O_{2\pm x}$ composition was divided into four parts and each portion calcined for 24 h in air at a different temperature. The calcination temperatures were 600, 700, 800 and 900° C. The X-ray diffractograms for the powder heated at 600° C showed broad fluorite peaks which became progressively sharper with increase in the calcination temperature. The surface area of all four powders was determined by the BET method and grain size distribution by scanning electron microscopy. Fine pastes of 25 wt % PtO_2 + 75 wt % of (U, M)$O_{2\pm x}$ solid solution in tri-ethylene glycol were prepared by grinding each powder mixture with 25 vol % solution of tri-ethylene glycol in ethanol until the ethanol had evaporated. This procedure was repeated several times. In addition, two pastes of composition, 85 wt % $(U_{0.38}Sc_{0.62})O_{2\pm x}$ + 15 wt % PtO_2 and 65 wt % $(U_{0.38}Sc_{0.62})O_{2\pm x}$ + 35 wt % PtO_2 were also prepared in order to study the effect of PtO_2 on the sensor performance. X-ray diffraction on a number of PtO_2-containing pastes heated to 600° C in air showed that the PtO_2 had decomposed to platinum without reacting with (U, M)$O_{2\pm x}$ fluorite solid solutions. Platinum electrodes were prepared from Hanovia Liquid

Table 1. The details of electrode preparation

Nomenclature	*Electrode composition*	*Calcination temperature of* $(U, M)O_{2\pm x}$, $T°C$ *(time, h)*
A1	75 wt % $(U_{0.4}Sc_{0.6})O_{2\pm x}$ + 25 wt % PtO_2	820 (24)
A2	75 wt % $(U_{0.4}Y_{0.6})O_{2\pm x}$ + 25 wt % PtO_2	700 (15)
A3	75 wt % $(U_{0.4}Dy_{0.6})O_{2\pm x}$ + 25 wt % PtO_2	600 (15)
A4	75 wt % $(U_{0.4}Pr_{0.6})O_{2\pm x}$ + 25 wt % PtO_2	600 (24)
B1	75 wt % $(U_{0.5}Y_{0.5})O_{2\pm x}$ + 25 wt % PtO_2	700 (15)
B2	75 wt % $(U_{0.4}Y_{0.6})O_{2\pm x}$ + 25 wt % PtO_2	700 (15)
B3	75 wt % $(U_{0.3}Y_{0.7})O_{2-x}$ + 25 wt % PtO_2	700 (15)
C1	75 wt % $(U_{0.4}Pr_{0.6})O_{2\pm x}$ + 25 wt % PtO_2	600 (24)
C2	75 wt % $(U_{0.4}Pr_{0.6})O_{2\pm x}$ + 25 wt % PtO_2	700 (24)
C3	75 wt % $(U_{0.4}Pr_{0.6})O_{2\pm x}$ + 25 wt % PtO_2	800 (24)
D1	85 wt % $(U_{0.38}Sc_{0.62})O_{2\pm x}$ + 15 wt % PtO_2	820 (24)
D2	75 wt % $(U_{0.38}Sc_{0.62})O_{2\pm x}$ + 25 wt % PtO_2	820 (24)
D3	65 wt % $(U_{0.38}Sc_{0.62})O_{2\pm x}$ + 35 wt % PtO_2	820 (24)
E1	Pt paste 8907	
E2	Pt paste 6082	
E3	Chloroplatinic acid	
E4	75 wt % $(U_{0.38}Sc_{0.62})O_{2\pm x}$ + 25 wt % PtO_2	900 (15)

Gold pastes 6082 and 8907 and by the *in situ* decomposition of chloroplatinic acid. Table 1 shows details of electrode composition, calcination temperature of $(U, M)O_{2\pm x}$ and the nomenclature of the electrodes.

2.3. *Preparation of sensors*

Complete sensors were prepared by painting the electrode under test (i.e. pure platinum or a composite consisting of PtO_2 and $(U, M)O_{2\pm x}$ fluorite solid solution). The sensor bodies after applying electrodes were slowly heated to 600° C in order to remove organics and in the case of composite electrodes also to decompose PtO_2 to platinum. The connections to the external and internal electrodes were made by a platinum wire and platinum leg of the Pt–Pt 13 % Rh thermocouple respectively as shown in Fig. 2. In most of the sensor tests a platinum spiral was placed in between the thermocouple bead and the inner electrode to ensure the integrity of the film. Without this platinum spiral, the thermocouple bead was occasionally observed to rupture the inner electrode film, thereby making a direct contact with the electrolyte.

2.4. *Sensor tests*

The sensors were slowly heated to 600° C with air at both electrodes and left at this temperature for ~ 100 h, prior to testing. The various tests consisted of the following:

(a) the determination of the open circuit e.m.f. with air at both electrodes and air (reference gas) at the internal and O_2–N_2 mixtures (0.1 to 100% O_2) at the external electrode;

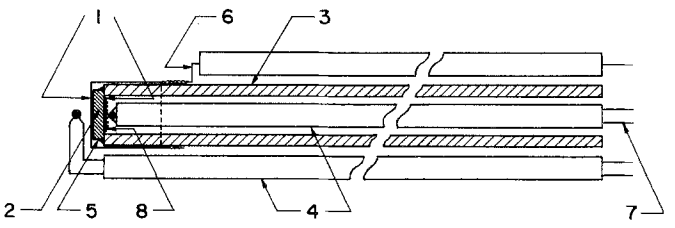

Fig. 2. A schematic diagram of the sensor assembly. (1) Electrode, (2) electrolyte, (3) alumina tube, (4) type R thermocouple, (5) weld junction, (6) external platinum wire connection, (7) internal platinum wire connection–Pt leg of the Pt–Pt 13% Rh thermocouple, (8) platinum spiral.

(b) the effect on the cell e.m.f. between 300 and 450° C of varying the internal flow rate by an order of magnitude;
(c) the effect on the cell e.m.f. of interchanging internal and external gases, and
(d) resistance measurements with air at both electrodes or air at the internal and O_2–N_2 mixtures at the external electrode.

Most of these tests were performed at 25 to 50° C intervals between 300 and 600° C during the cooling and subsequent heating cycle at 45 to 60 min time intervals. The oxygen partial pressure around the outer electrode was changed only at 600° C and the cell e.m.f. was allowed to settle for a minimum period of 15 h before recording further data. The tests described above were repeated for some sensors after they had been heat treated, first at 750° C ($\sim$ 100 h) and then at 900° C (60 to 100 h).

The open circuit e.m.f. was measured with either a high input impedance ($10^9\,\Omega$) digital multimeter or an electrometer (input impedance $> 10^{14}\,\Omega$). With air as the test gas, the total cell resistance was measured by passing a constant current (in the nA to μA range depending on the sensor temperature) through the sensor and measuring the equilibrium potential. In other test gases the cell resistance was measured by shorting the electrodes through an external load. In addition, complex impedance measurements were made on several cells using a Solartron frequency response analyser.

Typical flow rate for the internal electrode (effective tube volume 3 to 4 cm^3) was 180 $cm^3\,h^{-1}$ and for the external electrode (the effective work tube volume 650 cm^3), 1500 $cm^3\,h^{-1}$. In order to study the effect of flow rate on open circuit e.m.f. the internal flow rate was increased by up to an order of magnitude and the e.m.f. monitored. The effect of interchanging external and internal gases (air/1% O_2 in N_2) was studied between 300 to 400° C for urania-based electrodes and 400 to 500° C for porous platinum electrodes. The change in e.m.f. was recorded as a function of time. The flow rates for the internal and external electrodes were 180 and 1500 $cm^3\,h^{-1}$ respectively.

Although these tests are not exhaustive, they nevertheless provide useful information regarding the suitability of a material as a low temperature sensor electrode.

3. Results and discussion

All sensors based on (U, M)$O_{2\pm x}$ solid solutions contained PtO_2. The addition of PtO_2 was necessary for better adherence of electrode pastes to the electrolyte surface. In the sections to follow Figs 3, 4 and 7 to 9 show e.m.f. versus temperature curves for one representative gas composition (for a group of electrodes). Similar behaviour to that reported in these figures was observed for other O_2–N_2 gas mixtures. In Figs 3, 4, 7 to 9 the solid lines represent the theor-

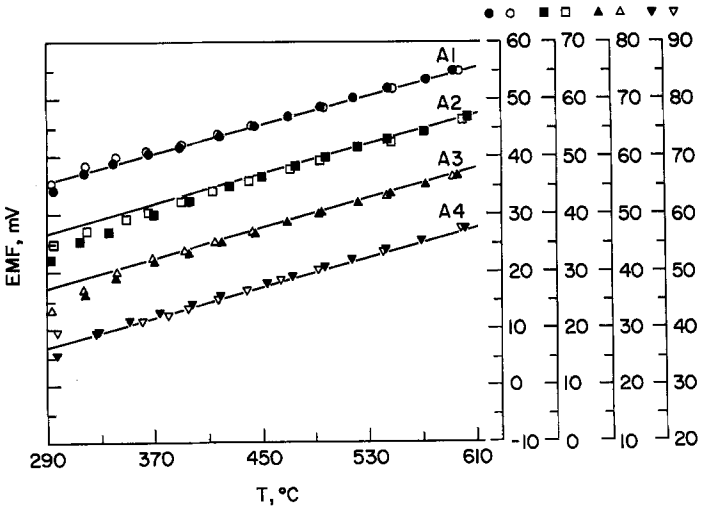

Fig. 3. E.m.f. versus temperature plots for electrodes of composition 75 wt % $(U_{0.4}M_{0.6})O_{2\pm x}$ + 25 wt % PtO_2 in air versus 1% O_2 in N_2. M = Sc (●○-Al), Y (■□-A2), Dy (▲△-A3), Pr (▼▽-A4). ●■▲▼-cooling, ○□△▽-heating cycle.

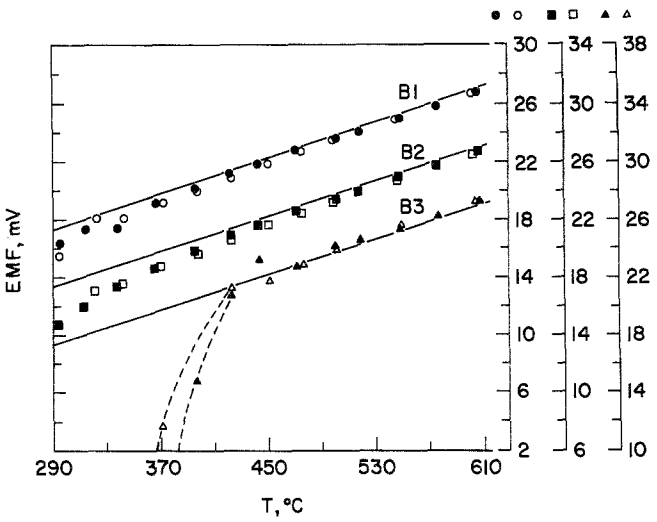

Fig. 4. E.m.f. versus temperature plots for electrodes of composition 75 wt % (U, Y)$O_{2\pm x}$ + 25 wt % PtO_2 in air versus 5.01% O_2 in N_2. U/Y ratio = 0.5/0.5 (●○-B1), 0.4/0.6 (■□-B2), 0.3/0.7 (▲△-B3). ●■▲-cooling, ○□△-heating cycle.

etical values calculated from the Nernst equation, the closed symbols represent the cooling and open symbols the heating cycle data. In these figures plots for each electrode have been offset from each other in the vertical (e.m.f.) axis for the sake of clarity. The failure of a sensor is characterized by the breakdown temperature (a temperature below which experimental e.m.f. deviate by more than 2.5 mV from the theoretical values). The ± 2.5 mV offset for most of the gas compositions and temperatures corresponds to about $\pm$ 10% (or less) error in oxygen concentration measurements.

3.1. *Electrodes based on (U, M)$O_{2\pm x}$ solid solutions*

3.1.1. Effect of dopant concentration and type. The dopants (M) studied were Sc, Y, Dy and Pr in order of increasing ionic radii for M^{3+}. Fig. 3 compares the response of four sensors, each one provided with a composite electrode material consisting of 75 wt % $(U_{0.4}M_{0.6})O_{2\pm x}$ (M = dopant) + 25 wt % PtO_2 as a function of temperature for air versus 1% O_2 in N_2. Although all sensors performed reasonably well down to 350° C, the overall behaviour of the sensor provided with electrodes based on urania–scandia solid solution (smallest dopant cation size) was better than the others.

Fig. 4 shows the performance of three sensors for air versus 5.01% O_2 in N_2 provided with urania–yttria based electrodes for which U/Y ratio was diferent (B1–B3). All three (U, Y)$O_{2\pm x}$ compositions were calcined under identical conditions to produce electrode powders with comparable grain size distribution. The sensors with electrodes B1 and B2 gave Nernstian e.m.f. down to 325 to 350° C (< 2 mV offsets); however, the sensor with electrode B3 (U/Y = 0.3/0.7) showed large deviations below about 425° C. Moreover, this sensor showed the largest cell resistance (of this group of sensors). Here it should be pointed out that in $(U_{0.3}Y_{0.7})O_{2-x}$ from which electrode B3 was prepared, the average oxidation state of uranium is six in air and that this material is oxygen deficient [23]. The normal mechanism of oxidation/reduction reaction at the gas/electrode interface (which is believed to be one of the major reasons for the better behaviour of (U, M)$O_{2\pm x}$ fluorite solid solution electrodes [10, 16]) is less likely to be operative for $(U_{0.3}Y_{0.7})O_{2-x}$ and may explain the poor performance of the sensor provided with electrodes based on this material. The breakdown temperatures in various gases for this sensor were similar to those observed for sensors provided with porous platinum electrodes.

3.1.2. Effect of electrode surface area/grain size on sensor performance. Fig. 5 shows scanning electron micrographs of powders of composition $(U_{0.4}Pr_{0.6})O_{2\pm x}$ calcined at 600 and 900° C. A rough estimate of the grain size was made from these and higher magnification micrographs. The average grain size for the powder calcined at

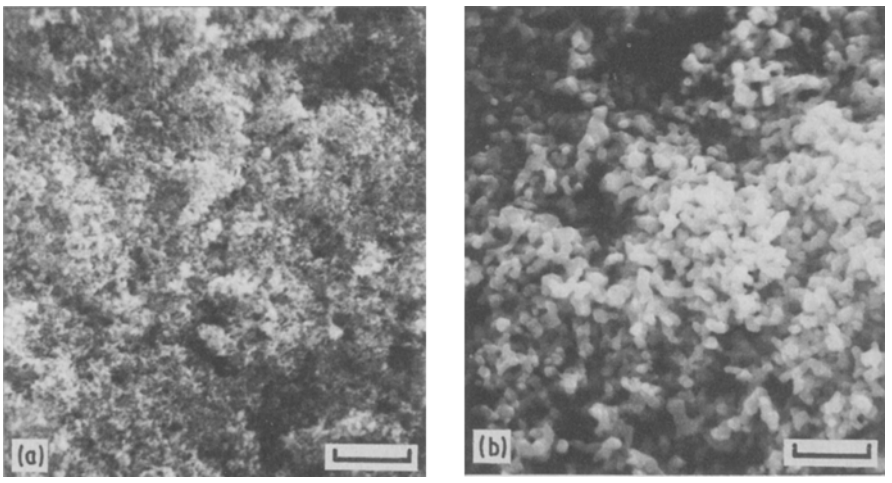

Fig. 5. Scanning electron micrographs of $(U_{0.4}Pr_{0.6})O_{2\pm x}$ powder after calcination in air (24 h) at (a) $-600°$, and (b) $-900°$ C. Bar = 0.6 μm.

600° C was approximately 0.02 to 0.03 μm whereas for the powder heated at 900° C it was in the range 0.1 to 0.3 μm. The results of surface area determinations are given in Table 2. The errors in these results are large especially for the powder calcined at 600° C but they nevertheless show a trend consistent with their respective scanning electron micrographs.

The *in situ* increase in the grain size of $(U_{0.4}Pr_{0.6})O_{2\pm x}$ seems to have little influence on the electrode resistance. This is shown in Fig. 6 for a $(U_{0.4}Pr_{0.6})O_{2\pm x}$/10 mol % Y_2O_3 + 90 mol % ZrO_2/$(U_{0.4}Pr_{0.6})O_{2\pm x}$ cell which was prepared by painting a paste of the largest surface area powder (600° C calcination) on both sides of the electrolyte disc. The total electrode resistance plotted in Fig. 6 was determined from impedance spectra first recorded in the 500 to 600° C temperature range after heat treating the cell at 600° C (50 h) and subsequently in the range 500 to 900° C after a further heat treatment at 900° C (50 h). Despite an increase in the grain size by nearly an order of magnitude, the electrode resistance decreased slightly, probably due to improved contact between the electrode and the electrolyte.

Since both powders calcined at 800 and 900° C had similar grain size and surface area, no sensor tests were performed with the latter powder. The results of open circuit e.m.f. measurements as a function of temperature for three sensors provided with electrodes for which $(U_{0.4}Pr_{0.6})O_{2\pm x}$ was calcined at 600 (C1), 700 (C2), and 800° C (C3) respectively are shown in Fig. 7 for air versus 5.01% O_2 in N_2. The sensor performance for all electrodes was reasonably good down to 330 to 360° C. The sensor with the C1 electrode (containing the $(U_{0.4}Pr_{0.6})O_{2\pm x}$ powder with the largest surface area) performed better than the others. The sensor with C1 electrode also had the lowest cell resistance over most of the temperature range over which sensible measurements could be made (400 to 600° C). The results of air versus 0.14% O_2 in N_2 for the sensor with C1 electrode are given in Table 3. The marginally better behaviour of the sensor provided with an electrode based on fine grain size $(U_{0.4}Pr_{0.6})O_{2\pm x}$ powder may be associated with its large surface area available for oxygen exchange reactions at the gas/electrode interface. Sensors provided with such electrode materials should respond quicker to changes in

Table 2. Results of surface area determination

Electrode composition	*Calcination conditions T° C (time, h)*	*Surface area ($m^2 gm^{-1}$)*
$(U_{0.4}Pr_{0.6})O_{2\pm x}$	600 (24)	39 ± 5
$(U_{0.4}Pr_{0.6})O_{2\pm x}$	700 (24)	17 ± 2
$(U_{0.4}Pr_{0.6})O_{2\pm x}$	800 (24)	9.5 ± 1
$(U_{0.4}Pr_{0.6})O_{2\pm x}$	900 (24)	9.3 ± 1

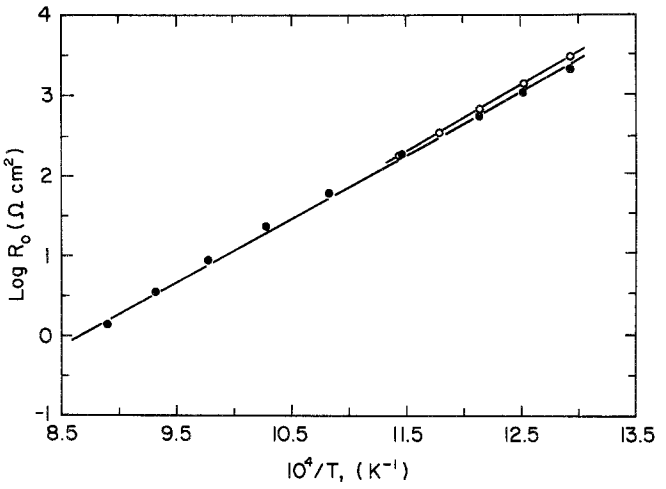

Fig. 6. Arrhenius plots for the electrode resistance of cell $(U_{0.4}Pr_{0.6})O_{2\pm x}$/10 mol % Y_2O_3 + 90 mol % ZrO_2/$(U_{0.4}Pr_{0.6})O_{2\pm x}$ after heat treatments at ○ −600° C and ● −900° C in 100% oxygen.

Table 3. E.m.f. data for 75 wt % $(U_{0.4}Pr_{0.6})O_{2\pm x}$ + 25 wt % PtO_2 electrode (600° C calcination) for air versus 0.14% O_2 in N_2

T° C	E(experimental*) (mV)	E(theoretical) (mV)
598.3	93.98	94.00
567.5	90.67	90.68
540.9	87.84	87.81
524.0	86.07	85.98
494.0	82.79	82.75
467.1	79.96	79.85
432.0	75.94	76.06
398.7	72.35	72.47
374.1	69.90	69.81
351.0	67.45	67.32
327.9†	66.42	64.83
293.7†	64.32	61.14
294.1†	67.70	61.19
320.8†	65.06	64.07
350.7	65.72	67.29
362.6	67.01	68.57
388.0	70.05	71.31
410.4	72.95	73.73
436.6	76.09	76.56
470.0	80.15	80.16
492.9	82.73	82.63
520.2	85.72	85.57
544.7	88.30	88.22
568.6	90.87	90.79
598.8	94.07	94.05

* Values not corrected for zero offset.
† E.m.f. drifts observed at these temperatures.

oxygen partial pressure and therefore should obtain equilibrium over a shorter time interval. In order to confirm this hypothesis an attempt was made to determine relative response rates by painting one side of zirconia–yttria discs with electrode C1 and the other with C3 and subjecting the discs to a gas atmosphere change from air to 1% O_2 in N_2 (and vice versa) at 425° C. However, the resulting change in voltage signal with time gave no clear indication of a marked difference in response rates.

3.1.3. Effect of PtO_2 addition on the sensor performance. Typical results of three sensors provided with electrodes of different PtO_2/$(U_{0.38}Sc_{0.62})O_{2\pm x}$ ratio are shown in Fig. 8 for air versus 1.01% O_2 in N_2. Despite the different amount of PtO_2 present all sensors performed well, down to about 350° C. The sensor with an electrode for which PtO_2/$(U_{0.38}Sc_{0.62})O_{2\pm x}$ ratio was 0.35/0.65 (D3) had the lowest resistance and its overall behaviour in various gas compositions was better than the others. It appears that the addition of PtO_2 (between 15 and 35 wt %) to the electrode material has only minor influence on the sensor performance. The sensors with composite electrodes containing platinum (added in the form of PtO_2) are sensitive to organic vapours and trace levels of CO in the flue gases [24] although their sensitivity is

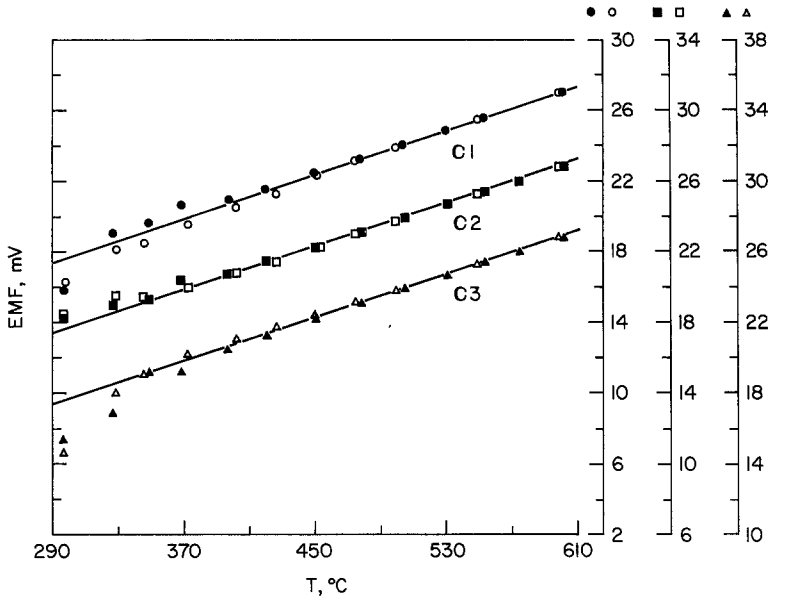

Fig. 7. E.m.f. versus temperature curves for electrodes of composition 75 wt % $(U_{0.4}Pr_{0.6})O_{2\pm x}$ + 25 wt % PtO_2 in air versus 5.01% O_2 in N_2. Surface area ($m^2\,gm^{-1}$) of $(U_{0.4}Pr_{0.6})O_{2\pm x}$ powder = 39 (●○-C1), 17 (■□-C2), and 9.5 (▲△-C3). ●■▲-cooling and ○□△-heating cycle.

far less marked in comparison with pure platinum electrodes.

3.2. *Platinum electrodes*

The results of open circuit e.m.f. measurements (air/air) as a function of temperature for four sensors provided with electrodes of platinum pastes 8907 (E1), 6082 (E2), chloroplatinic acid (E3) and 75 wt % $(U_{0.38}Sc_{0.62})O_{2\pm x}$ + 25 wt % PtO_2 (E4) after the 600° C heat treatment are shown in Fig. 9. All sensors with platinum electrodes gave significant errors below about 450° C whereas the sensor with $(U_{0.38}Sc_{0.62})O_{2\pm x}$-based electrode gave Nernstian e.m.f down to 300° C. Heat treatment of the sensors at 750 and 900° C resulted in deterioration in the performance of all sensors. The effect of heat treatment was more pronounced for platinum electrodes and the sensor with $(U_{0.38}Sc_{0.62})O_{2\pm x}$-based electrode performed satisfactorily down to 360° C even after the 900° C treatment. These observations on platinum electrodes are consistent with those of other authors [6].

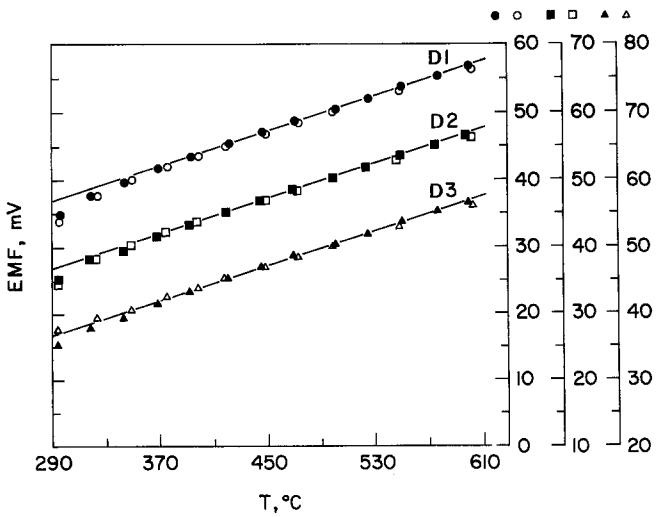

Fig. 8. E.m.f. versus temperature curves for electrodes where composition = l wt % $(U_{0.38}Sc_{0.62})O_{2\pm x}$ + (100 − l) wt % PtO_2 in air versus 1% O_2 in N_2. l = 85 (●○-D1), 75 (■□-D2), 65 (▲△-D3). ●■▲-cooling and ○□△-heating cycle.

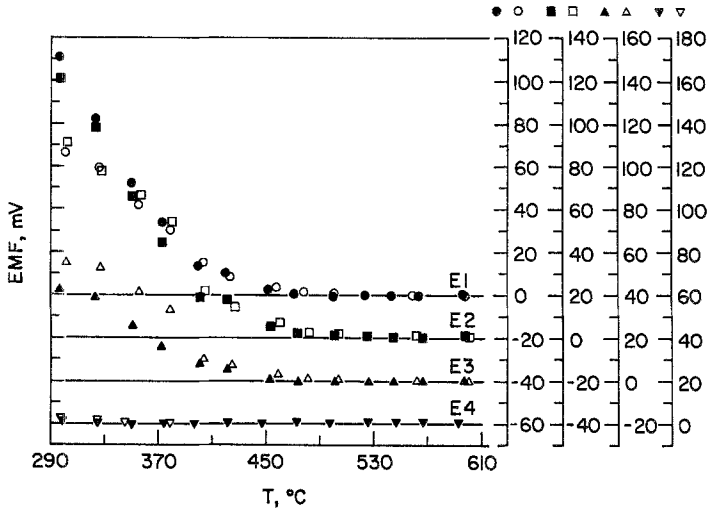

Fig. 9. E.m.f. versus temperature curve in air versus air for electrodes: platinum paste 8907 (●○-E1), platinum paste 6082 (■□-E2), chloroplatinic acid (▲△-E3) and 75 wt % $(U_{0.38}Sc_{0.62})O_{2\pm x}$ + 25 wt % PtO_2 (▼▽-E4). ●■▲▼-cooling and ○□△▽-heating cycle.

3.3. *Effect of flow rate and interchanging internal and external gases*

For both urania-based and porous platinum electrodes the effect of flow rate was more pronounced below the breakdown temperature which was about 350° C for urania-based and ~450° C for platinum electrodes. Increasing the flow rate led to both positive or negative deviations from the Nernstian values and these deviations were much higher for platinum electrodes. Amongst urania-based electrodes minimum flow rate dependence was observed for $(U_{0.38}Sc_{0.62})O_{2\pm x}$-based electrodes, whereas for platinum electrodes the best behaviour was observed for that prepared by the *in situ* decomposition of chloroplatinic acid.

On interchanging gases between external and internal electrode compartments, the e.m.f. recovered to the Nernstian values at temperatures as low as 350° C for $(U_{0.38}Sc_{0.62})O_{2\pm x}$-based electrodes whereas for platinum electrodes errors were rather large even at 450° C. Moreover, urania-based electrodes responded very rapidly to the oxygen partial pressure changes compared with porous platinum electrodes. Although these tests were rather qualitative, they nevertheless demonstrate the superior characteristics of urania-based electrodes over platinum.

3.4. *Sensor resistance and effect of heat treatment*

The resistance as measured by d.c. techniques includes both electrode and electrolyte contributions. Typical resistance values for all types of electrodes used varied between 1500 to 6000 Ω at 600° C and 70 to 500 kΩ at 400° C. Even for the same electrode material, the total resistance varied from sensor to sensor because of (i) the difficulty of reproducing the same electrode/electrolyte contact area, and (ii) the electrolyte resistance itself was different for different sensors. Thus on the basis of d.c. resistance measurements it was not possible to make valid comparison between various electrodes. However, complex impedance measurements on electrode/4.7 ScZAl/electrode cells where both electrodes were exposed to either air or 100% oxygen indicate that at 600° C, the major contribution to the total sensor resistance was made by the electrolyte. At lower temperatures (400° C or below) the electrode contribution was significant and it increased further with decreasing temperature (Fig. 10). In general, the electrode resistance of urania-based electrodes was lower than porous platinum. The difference increased substantially when the electrodes were heat treated at temperatures higher than 600° C. For example Fig. 11 shows electrode arcs for two

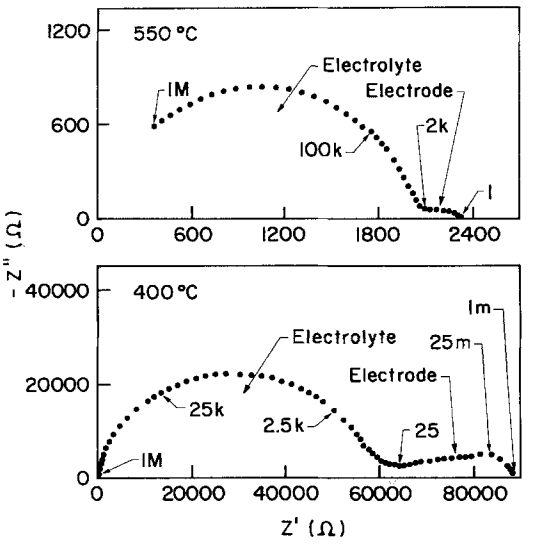

Fig. 10. Impedance spectra of a typical sensor (with electrodes Al and electrolyte 50 wt % (4.7 mol % Sc_2O_3 + 95.3 mol % ZrO_2) + 50 wt % Al_2O_3) in air at two temperatures showing relative electrode and electrolyte contributions. The numbers on the arcs represent frequencies in Hz.

sensors, one prepared with platinum paste 6082 and the other with 75 wt % $(U_{0.38}Sc_{0.62})O_{2\pm x}$ + 25 wt % PtO_2 on Viking 7 mol % Y_2O_3 + 93 mol % ZrO_2 (YSZ-7) tubes, at 500° C after the sensors were heat treated, first at 600° C and then at 900° C. High temperature heating had little influence on the electrode resistance of urania–scandia based electrodes but the resistance of platinum electrodes deteriorated markedly. The increase in the electrolyte resistance (more obvious on the expanded scale of Fig. 11b) due to high temperature heat treatment is a characteristic property of the Viking electrolyte composition. Similar behaviour was observed for sintered (1850° C) bars (4 probe d.c. data) which were prepared from Viking powder of 7 mol % Y_2O_3 + 93 mol % ZrO_2 composition.

For the electrolyte (4.7 ScZAl) used in this work, less than 35% of the electrode/electrolyte contact area is available for oxygen exchange reactions because of the presence of ~ 60 vol % (50 wt %) of the insulator Al_2O_3 phase and some porosity. In order to increase the useful electrode/electrolyte contact area, a thin film (~ 20 μm) of prereacted Al_2O_3-free Sc_2O_3–ZrO_2 composition was cosintered [25] on both flat surfaces of 4.7 ScZAl discs. Sensors prepared from such electrolyte samples had much lower electrode resistance (by a factor of ~ 3 to 4). This feature was particularly useful for performance tests at low temperatures as such sensors were less prone to noise pick-up and gave stable e.m.f. compared with our normal sensors.

3.5. *Sensor electrolyte resistance*

The electrolyte composition (4.7 ScZAl) used in these sensor tests is slightly understabilized and

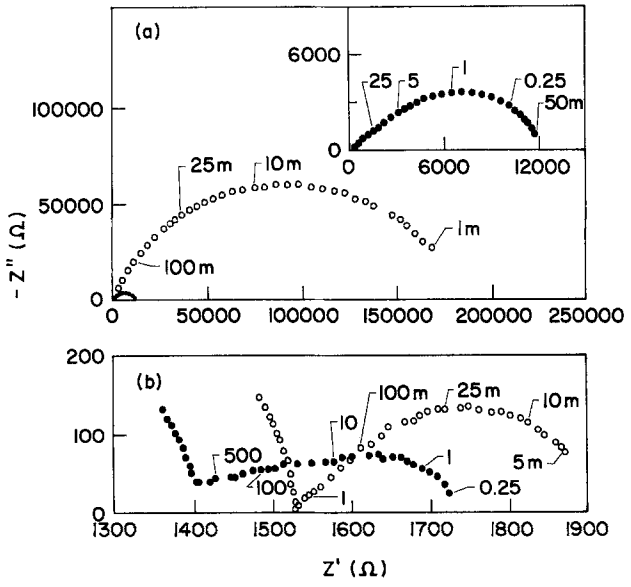

Fig. 11. Impedance spectra for two 7 mol % Y_2O_3 + 93 mol % ZrO_2 (Viking) tube sensors at 500° C (air versus air) provided with electrodes: platinum paste 6082 (a) and 75 wt % $(U_{0.38}Sc_{0.62})O_{2\pm x}$ + 25 wt % PtO_2 (b) after heat treatments at 600° C (●) and 900° C (○). The numbers on the arcs represent frequencies in Hz.

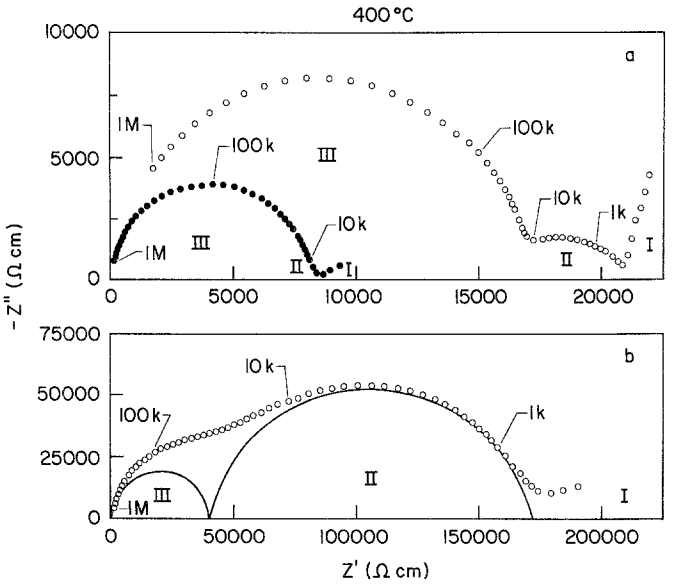

Fig. 12. Impedance spectra at 400° C in 100% oxygen for (a) o-10 mol % Y_2O_3 + 90 mol % ZrO_2, ●-8 mol % Sc_2O_3 + 92 mol % ZrO_2 and (b) 50 wt % (4.7 mol % Sc_2O_3–ZrO_2) + 50 wt % Al_2O_3. Arcs I, II and III represent electrode, grain boundary and volume contributions respectively. The numbers on the arcs are frequencies in Hz.

contains monoclinic zirconia (m-ZrO_2) in addition to the 50 wt % Al_2O_3. Both the presence of m-ZrO_2 and Al_2O_3 have a detrimental influence on the conductivity. The m-ZrO_2, in addition to reducing conductivity, introduces jumps and hysteresis effects in the Arrhenius plots due to the martensitic monoclinic/tetragonal transformation [20]. The electrolyte discs also develop microcracks during thermal cycling resulting in increased resistivity. Fig. 12 shows a typical impedance plot of 4.7 ScZAl electrolyte at 400° C. Included for comparison in this figure are the data for 8 mol % Sc_2O_3 + 92 mol % ZrO_2 and 10 mol % Y_2O_3 + 90 mol % ZrO_2. The electrical conductivity of our electrolyte is lower by an order of magnitude compared with pure electrolyte materials. It is also obvious from Fig. 12 that the major contribution to the total resistivity in 4.7 ScZAl comes from the grain boundaries. The grain boundary contribution varies with the method of preparation of the electrolyte and the total conductivity is a complex function of the electrolyte microstructure [21].

4. Conclusions

So far more than 40 sensors have been tested in this laboratory and almost all the sensors with (U, M)$O_{2\pm x}$-based electrodes performed satisfactorily down to 350° C and over the oxygen concentration range of 100 to 0.1% O_2. Sensors with pure platinum electrodes, however, showed large deviations from Nernstian behaviour below about 450° C. In general, composite electrodes based on (U, M)$O_{2\pm x}$ had much lower electrode resistance and time constant than platinum. Moreover, urania-based electrodes were far less sensitive to variations in the flow rates of gases and responded rapidly to oxygen partial pressure changes in comparison with the platinum electrodes. Drifts in e.m.f. were commonly observed for all electrodes at low temperatures but for nonstoichiometric oxide electrodes they were obvious only below about 350° C. The sensors with urania–scandia electrodes showed much better stability with respect to time at lower temperatures. The fact that the sensors with (U, M)$O_{2\pm x}$ electrodes produced Nernstian behaviour at lower temperatures – despite the use of an electrolyte material with at least an order of magnitude lower conductivity, than can be expected from pure materials – is a good indication of the relatively important role played by the electrodes. The better behaviour of (U, M)$O_{2\pm x}$ electrodes is associated with their ability to rapidly exchange oxygen at the gas/electrode interface. The sensors with urania-based electrode materials are now undergoing extensive plant trials to assess their suitability and durability in industrial environments.

Acknowledgements

The authors wish to thank Ms B. Terrell, Mr B. A. Pattinson and Mr R. Sherwood for experimental assistance. The authors are also grateful to Mr W. G. Garrett and Drs M. J. Bannister, M. J. Murray and J. Drennan for many useful discussions. The manuscript was critically reviewed by Mr W. G. Garrett.

References

[1] D. E. Williams and P. McGeehin, 'Electrochemistry', Vol. 9 (The Royal Society of Chemistry, London, 1984) p. 246.
[2] 'Chemical Sensors', Proceedings of the International Meeting on Chemical Sensors, Fukuoka, Japan, September 19–22, edited by T. Seiyama, K. Fueki, J. Shiokawa and S. Suzuki (Elsevier, Amsterdam, 1980).
[3] 'Measurement of Oxygen', Proceedings of an Interdisciplinary Symposium, Demark, 26–27 September 1974, edited by H. Degn, I. Balslev and R. Brook (Elsevier, Amstrdam, 1976).
[4] H. J. de Bruin and S. P. S. Badwal, *J. Aust. Ceram. Soc.* **14** (1978) 20.
[5] J. E. Bauerle, *J. Phys. Chem. Solids* **30** (1969) 2657.
[6] R. T. Dirstine, W. O. Gentry, R. N. Blumenthal and W. Hammetter, *Ceram. Bull.* **58** (1979) 778.
[7] T. Takahashi, T. Esaka and H. Iwahara, *J. Appl. Electrochem.* **7** (1977) 303.
[8] S. P. S. Badwal, F. T. Ciacchi and A. S. Kashmirian, Abstracts of Sixth Australian Electrochemistry Conference, Geelong, Australia, February 19–24, 1984.
[9] S. P. S. Badwal and F. T. Ciacchi, submitted to *Solid State Ionics*.
[10] S. P. S. Badwal, M. J. Bannister and M. J. Murray, *J. Electroanal. Chem.* **168** (1984) 363.
[11] D. M. Haaland, *J. Electrochem. Soc.* **127** (1980) 796.
[12] W. J. Fleming, *ibid.* **124** (1977) 21.
[13] J. E. Anderson and Y. B. Graves, *ibid.* **128** (1981) 294.
[14] L. Hayne and D. den Engelsen, *ibid.* **124** (1977) 727.
[15] S. P. S. Badwal, *J. Electroanal. Chem.* **146** (1983) 425.
[16] *Idem, ibid.* **161** (1984) 75.
[17] S. P. S. Badwal, M. J. Bannister and W. G. Garrett, 'Advances in Ceramics', Vol. 12, edited by M. Rühle, N. Claussen and A. H. Heuer, (The American Ceramics Society Inc., Columbus, Ohio, 1984) p. 598.
[18] M. J. Bannister, N. A. McKinnon and R. R. Hughan, US Patent No. 4193 857 (1980).
[19] M. J. Bannister, W. G. Garrett, K. A. Johnston, N. A. McKinnon, R. K. Stringer and H. S. Kanost, 'Materials Science Monographs', Vol. 6, edited by P. Vincenzini (Elsevier, Amsterdam, 1980) p. 211.
[20] S. P. S. Badwal, *J. Aust. Ceram. Soc.* **18** (1982) 35.
[21] S. P. S. Badwal and J. Drennan, *J. Aust. Ceram. Soc.* **20** (1984) 28.
[22] W. G. Garrett, Proceedings of the 10th Australian Ceramic Society Conference, Melbourne, Australia, August 24–27, 1982, p. 339.
[23] E. A. Aitken and R. A. Joseph, *J. Phys. Chem.* **70** (1966) 1090.
[24] S. P. S. Badwal, M. J. Bannister, F. T. Ciacchi, W. G. Garrett, A. S. Kashmirian and R. C. Wotherspoon, Proceedings of the 11th Australian Ceramic Society Conference, Sydney, Australia, August 29–31, 1984, p. 103.
[25] S. P. S. Badwal, *J. Appl. Electrochem.* **14** (1984) 379.